# Complex I deficiency due to loss of Ndufs4 in the brain results in progressive encephalopathy resembling Leigh syndrome

Albert Quintana[a,1], Shane E. Kruse[a,1], Raj P. Kapur[b], Elisenda Sanz[c], and Richard D. Palmiter[a,2]

[a]Howard Hughes Medical Institute and Department of Biochemistry, University of Washington, Seattle, WA 98195; [b]Department of Laboratories, Seattle Children's Hospital, Seattle, WA 98105; and [c]Department of Pharmacology, University of Washington, Seattle, WA 98195

Contributed by Richard D. Palmiter, May 5, 2010 (sent for review April 22, 2010)

**To explore the lethal, ataxic phenotype of complex I deficiency in Ndufs4 knockout (KO) mice, we inactivated Ndufs4 selectively in neurons and glia (NesKO mice). NesKO mice manifested the same symptoms as KO mice including retarded growth, loss of motor ability, breathing abnormalities, and death by ∼7 wk. Progressive neuronal deterioration and gliosis in specific brain areas corresponded to behavioral changes as the disease advanced, with early involvement of the olfactory bulb, cerebellum, and vestibular nuclei. Neurons, particularly in these brain regions, had aberrant mitochondrial morphology. Activation of caspase 8, but not caspase 9, in affected brain regions implicate the initiation of the extrinsic apoptotic pathway. Limited caspase 3 activation and the predominance of ultrastructural features of necrotic cell death suggest a switch from apoptosis to necrosis in affected neurons. These data suggest that dysfunctional complex I in specific brain regions results in progressive glial activation that promotes neuronal death that ultimately results in mortality.**

cerebellum | mitochondria | gliosis | neurodegeneration | vestibular nucleus

Neural pathologies frequently result from dysfunctional mitochondria, and Leigh syndrome (LS) is a common clinical phenotype (1). LS, or subacute necrotizing encephalopathy, is a progressive neurodegenerative disorder (2) affecting 1 in 40,000 live births (3). LS is regarded as the most common infantile mitochondrial disorder, and most patients exhibit symptoms before 1 mo of age (4, 5). Several cases of adult-onset LS have also been reported recently (6–10). In vivo imaging techniques such as MRI reveal bilateral hyperintense lesions in the basal ganglia, thalamus, substantia nigra, brainstem, cerebellar white matter and cortex, cerebral white matter, or spinal cord of LS patients (6, 11–14). The lesions usually correlate with gliosis, demyelination, capillary proliferation, and/or necrosis (10, 15). Behavioral symptoms of LS patients can include (with a wide variety of clinical presentation) developmental retardation, hypotonia, ataxia, spasticity, dystonia, weakness, optic atrophy, defects in eye or eyelid movement, hearing impairment, breathing abnormalities, dysarthria, swallowing difficulties, failure to thrive, and gastrointestinal problems (4–6, 16, 17). The cause of death in most LS cases is unclear, and the lack of a genetic model to study the disease progression and cause of death has impeded the development of adequate treatment. Prognosis for LS (and most diseases resulting from mitochondrial dysfunction) is very poor; there is no cure and treatment is often ineffective (5). Thus, a murine model of this disease should allow a better means of studying the mechanism(s) underlying the encephalopathy and should allow a more facile investigation of potential therapies.

## Results

**Mice Lacking Ndufs4 in Nervous System Resemble Total Knockout.** Mice lacking Ndufs4 (Ndufs4 KO) in all cells develop a complex phenotype and die by postnatal day 50 (P50) (18). Mice with at least one intact *Ndufs4* allele are indistinguishable from WT mice, and they are sometimes used interchangeably with WT as controls (CT). To examine the role of the CNS in pathology, we restricted the inactivation of *Ndufs4* gene to neurons and astroglial cells by crossing the $Ndufs4^{lox/lox}$ mice with mice expressing Cre recombinase from the *Nestin* locus (19) to create mice that we refer to as NesKO mice. We confirmed that *Nestin-Cre* results in recombination primarily in the CNS by crossing the mice with a Rosa26-reporter line and by PCR analysis of DNA isolated from various organs (Fig. S1*A*). These data agree with the known robust expression of *Nestin* in the mouse brain with lower levels in a few cell types in heart, kidney, lung, pancreas, and testes (19).

**Complex I Activity Is Depressed in Brain of NesKO Mice.** Enriched mitochondria were prepared from liver and brain to measure respiratory capacity. Normal rotenone-sensitive complex I activity was detected in submitochondrial particles (SMPs) isolated from liver of NesKO or CT mice; however, complex I activity was very low or absent in SMPs derived from NesKO brain tissue compared with CT (Fig. S1*B*). Complex I–dependent $O_2$ consumption by brain tissue from NesKO mice was depressed ∼50% compared with that in CT mice, whereas complex II and IV activities were unaffected (Fig. S1 *C* and *D*). The loss of complex I activity was independent of the age of the mouse. These results with NesKO mice are identical to those observed in the brains of total KO mice (18).

**Nearly Identical Phenotype of KO and NesKO Mice.** NesKO mice had a phenotype similar to that of total KO mice (18). By postnatal day 21 (P21), most NesKO mice were smaller than control littermates and reached a maximum body weight of ∼12 g at ∼P30 (Fig. S1*E*). Resting body temperature of NesKO mice was ∼2 °C lower than controls after P30 (Fig. S1*F*). NesKO mice occasionally experienced cataracts, ptosis, or optic atrophy. Even when their eyes appeared normal, the mice often had defective visual acuity as measured by Morris water maze, visual cliff test, and visual placing (Fig. S1*G*). However, even KO mice with defective vision were able to distinguish light from dark (Fig. S1*H*). Starting at ∼P35, NesKO mice developed severe ataxia: they had splayed legs, became unresponsive to a firm nudge, were slow and awkward at righting themselves, and sometimes became so unstable they would lose their balance and fall over.

Author contributions: A.Q., S.E.K., and R.D.P. designed research; A.Q., S.E.K., R.P.K., and E.S. performed research; A.Q., S.E.K., R.P.K., and E.S. analyzed data; and A.Q., S.E.K., and R.D.P. wrote the paper.

The authors declare no conflict of interest.

Freely available online through the PNAS open access option.

[1]A.Q. and S.E.K. contributed equally to this work.

[2]To whom correspondence should be addressed. E-mail: palmiter@u.washington.edu.

This article contains supporting information online at www.pnas.org/lookup/suppl/doi:10.1073/pnas.1006214107/-/DCSupplemental.

NesKO mice >P40 were unable to maintain balance on a 7-mm-wide ledge, failed a negative geotaxis test, attempted to clasp a hind leg when suspended by their tail, and fell from a rotating rod very quickly, in contrast to CT mice (Fig. S1*I*). NesKO mice were very submissive and rarely vocalized even when stressed by handling, tail clipping for genotyping, or in response to a toe pinch (percent vocalization during toe pinch assay: WT, 91.7%, $n = 12$, $P < 0.0001$; NesKO and KO, 18.0%, $n = 50$, $P < 0.0001$). Some NesKO mice had spontaneous tonic–clonic seizures (~1/20 NesKO and KO mice), whereas others developed seizures in response to handling (~1/10 NesKO and KO mice), and the frequency of seizures increased with disease progression. Intermittent breathing irregularities were detected as early as P14 and included hypo- or hyperventilation, but most often involved gasping activity. Between P35 and P50, the NesKO mice began to lose weight, their ataxia worsened, and they died shortly thereafter. The only significant difference between the phenotype of NesKO mice and complete KO mice is that the latter manifest a lag time between the exogenic phase of club hair growth and the anagenic phase of the next hair cycle, resulting in ~7-d period without hair or pigment (18), whereas NesKO mice had a normal hair cycle. An extensive summary of the phenotypes of KO and NesKO mice is provided in Table S1.

**Progression of Behavioral Phenotype.** Having established that the major features of the Ndufs4 KO pathology are of neurological origin, we set out to define the brain regions affected by the loss of Ndufs4 and to correlate pathological changes in the brain with progression of the behavioral phenotype. A scoring system was established based on weight gain, body temperature, various measures of locomotor skill and activity, touch response, and trunk curl, rather than age alone, to account for the asynchronous progression of the phenotype in different mice. Our 12-point scoring system (Table S2) classified KO or NesKO mice into either early (one to four points), middle (five to eight points), or late (nine to 12 points) stage of disease progression. These studies were performed with both KO and NesKO mice. KO mice in the early stage of disease (P18–P26) had nearly normal body weight and body temperature, did not display hind limb clasping, and suffered only mild ataxia. Middle-stage mice (P26–P38) usually had ~2 °C decrease in resting body temperature ($T_b$) with spontaneous hypothermic (>10 °C $T_b$ decrease) events, increased ataxia, and curled trunks and clasped hind limbs during tail suspensions, and ceased gaining weight. Late-stage mice (usually > P38) displayed severe ataxia, lethargy, >2 °C lower $T_b$ with spontaneous hypothermic (>10 °C $T_b$ decrease) events, and unstable body weight, and became less responsive to handling.

**Progression of Neuropathology in KO Mice.** Brain sections stained with H&E did not reveal any obvious differences between CT and KO mice at early stages (<P26) of disease. However, late-stage (>P38) NesKO and KO mice had conspicuous vacuolation (spongiform degeneration) within vestibular nuclei (VN) of the brainstem that was absent in CT mice (Fig. 1 *A–C*). Similar changes were present in the inferior olive (IO), fastigial nucleus (FN), caudal cerebellar vermis (nodulus and uvula), and olfactory bulb (OB). Furthermore, vascularity of the VN and posterior cerebellum in both KO and NesKO mice was greatly increased compared with CT mice, as highlighted by laminin immunostaining (Fig. 1 *D–F*). In conjunction with vascular proliferation, hemorrhagic foci were detected in the brainstem and occasionally the midbrain of some late stage KO and, more often, in NesKO mice (Fig. S2 *A–C*).

Astroglial and microglial reactivity are early and common features of neuropathology; therefore, we performed immunofluorescence with antibodies against GFAP (Fig. S2 *A–C*) and ionized calcium binding molecule 1 (Iba-1), respectively, to evaluate the progression of the disease in the affected areas and to correlate it

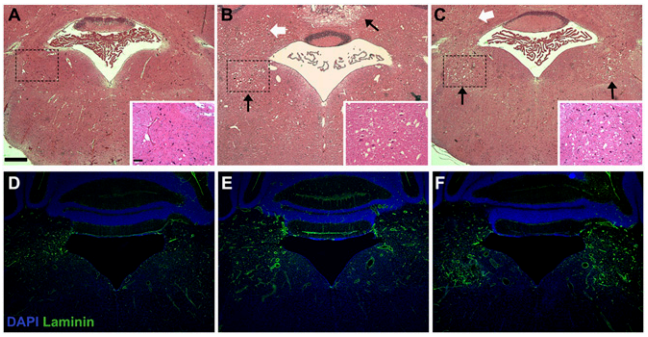


**Fig. 1.** Vacuolation and vascular proliferation in NesKO and KO mice. (*A*) No pathology is observed in H&E staining of brain sections of CT animals ($n = 5$). (*B* and *C*) In contrast, both late-stage NesKO (*B*, $n = 5$) and KO (*C*, $n = 5$) mice show marked vacuolation in the VN (black arrows; *Inset* shows higher magnification of indicated area) and, to a lesser extent, in deep cerebellar nuclei (white arrow). (*D–F*) Vascular proliferation, as assessed by laminin staining, was increased around the VN in NesKO (*E*) and KO (*F*) mice compared with CT (*D*). (Scale bar, *A–F*, 125 μm; *Inset*, 25 μm.)

with the behavioral score described (Table S2). Frozen brain sections from NesKO ($n = 5$) and KO mice ($n = 5$) at different stages, as well as CT mice ($n = 5$), were analyzed. A similar pattern of activation in astrocytes and microglial cells appeared simultaneously in the brains of NesKO and KO mice, with overt lesions in the areas where vacuolation was detected in H&E-stained sections. NesKO mice had a higher frequency of hemorrhages in midbrain, and of gliosis and spongiform lesions in the anterior cerebellum than KO mice. CT animals did not show astroglial activation and microglial cells retained a ramified morphology typical of a nonreactive status (Fig. S2 *D* and *E*). In contrast, hypertrophic Iba-1–positive microglial cells were detected in the OB and VN of early-stage KO mice, being more numerous in the former (Fig. 2 *A, D, G,* and *J*). By middle stage, activated microglial cells with highly reactive morphological changes (hypertrophy and thickened, short processes) were abundant in OB and VN and appeared in the posterior lobules of the cerebellar vermis (especially lobules VIII–X), deep cerebellar nuclei, and IO/gigantocellular/lateral reticular region (IO/Gi/LRt) (Fig. 2 *B, E, H,* and *K*). Enhanced microglial activation was observed in late-stage animals, where dense infiltrates were present, especially in the peri-glomerular outer plexiform layer of the OB (Fig. 2*C*), the posterior cerebellar vermis, and the medial/lateral VN where overt tissue damage was detected (Fig. 2 *F* and *I*). An increase in the number of Iba1-positive cells was also manifest in the IO and surrounding areas (gigantocellular region, parapyramidal region; Fig. 2*L*) and in the deep cerebellar nuclei (FN and interposed nuclei; Fig. 2*G*, arrows).

Because microglia can have both positive and detrimental roles in inflammatory processes, we further elucidated the relative contribution of microglia reactivity in the progression of the disease by using CD11b as a marker of phagocytic microglia (Fig. S3). CD11b-positive cells were absent in early-stage animals (Fig. S3 *A, D, G,* and *J*) but were visible in the OB, cerebellum, and VN of middle-stage animals (Fig. S3 *B, E,* and *H*). Late-stage animals showed abundant CD11b expression in all affected areas (Fig. S3 *C, F, I,* and *L*).

**Oxidative Stress, Caspase-8 Activation, and Neuronal Cell Death in KO Mice.** Glial reactivity is usually a result of neuronal cell death. To confirm the presence of neuronal loss in the affected areas, immunohistochemistry for NeuN (a neuronal marker) was performed in sections of control and late-stage KO mice. Confocal microscopy revealed a significant decrease in the NeuN-positive cells in all affected areas. Supporting these data, quantification

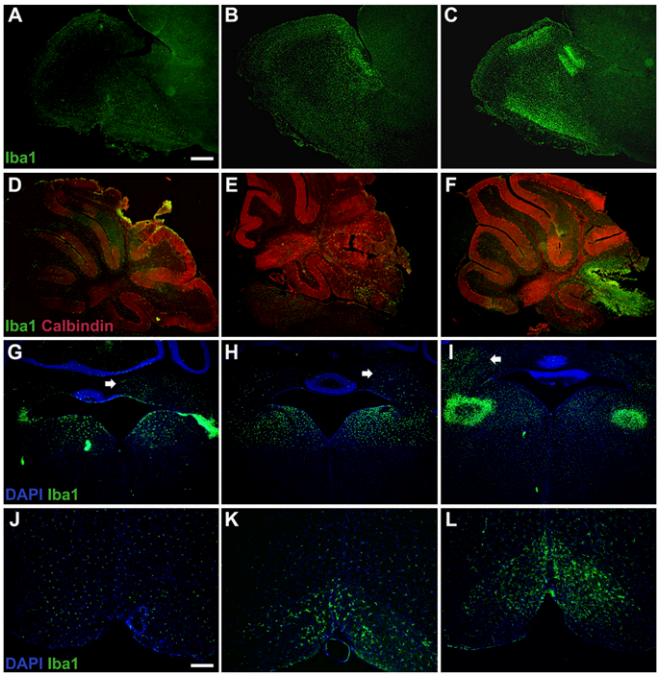


**Fig. 2.** Progressive inflammatory response in the brains of KO mice. (*A–C*) Microglial activation in the OB of KO mice at early (*A*), middle (*B*), or late (*C*) stage of the disease was determined using an antibody against Iba-1.(*D-F*) Calbindin and Iba-1 staining in the cerebellum of KO mice at early (*D*), middle (*E*), or late (*F*) stage of the disease. (*G–I*) Iba-1 staining in the vestibular and deep cerebellar nuclei of KO mice at early (*G*), middle (*H*), or late stage (*I*) of the disease. (*J–L*) Iba-1 staining in the IO of KO mice at early (*J*), middle (*K*), or late stage (*L*) of the disease. Iba-1 staining in the brains of KO mice at different stages of the disease (early, middle, and late stages; $n = 5$ each) shows a localized and progressive inflammatory response. In early-stage animals (*A, D, G,* and *J*), marked microglial activation is already present in the OB (*A*), VN (*G*), and deep cerebellar nuclei (*G*, arrow). However, no microglial response is visible in either the cerebellum (*D*) or in the vicinity of the IO (*J*). In middle-stage animals (*B, E, H,* and *K*), enhanced microglial accumulation is observed in the OB (*B*), VN (*H*), and, to a lesser extent, in the deep cerebellar nuclei (*H,* arrow), cerebellar lobes (*E*), and IO (*K*). In late-stage animals (*C, F, I, and L*), severe microglial activation is observed in the olfactory lobe (*C*) and the deep cerebellar nuclei (*I,* arrow). Extensive microglial reactivity along with localized tissue destruction is observed in the cerebellar lobes (*F*, where loss of calbindin staining is visible in the affected lobes) and VN (*I*). In contrast, only moderate activation is present surrounding the IO (*L*). (Scale bar, *A–I*.125 μm; *J–L*, 50 μm.)

of the number of NeuN-positive cells per area confirmed the disappearance of neurons in the cerebellum, OB, and VN of KO mice (Fig. 3 *A–I*).

To explore the mechanisms underlying neuronal death, the oxidation status of the proteins and activities of the initiators of the two main apoptotic pathways were assessed in the OB, the earliest and most affected area. Protein oxidation in CT and middle-stage KO mice was assessed in protein lysates by derivatization of carbonyls with 2,4-dinitrophenylhydrazine followed by antibody detection (Oxyblot analysis). Samples from KO mice showed increased protein oxidation when compared with CT mice (Fig. 4*A*). No signal was detected in nonderivatized controls. The activation of the initiator caspases of the extrinsic and intrinsic apoptotic pathways were assessed by Western blot analysis. There was a significant increase in the level of cleaved caspase-8 (the initiator caspase of the extrinsic pathway) in KO mice compared with CT mice, whereas the level of cleaved caspase-9 (the initiator caspase of the intrinsic mitochondrial pathway) was unaltered (Fig. 4*B*). The increased level of active caspase-8 correlates with a significant increase of the glial markers GFAP and Iba-1, suggesting that caspase-8 activation may be a result of the inflammatory state present in the affected areas.

Interestingly, very little caspase-3 activation was observed, except in the external plexiform layer of the OB (Fig. S4 *A* and *E*), at any time point studied. Furthermore, only scattered caspase 3–positive cells in the VN and cerebellar lobes were observed in KO mice (Figs. S4 *B, C, F,* and *G*) despite the clear loss of Purkinje cells (readily visualized by DAPI staining and loss of calbindin immunoreactivity coupled with massive infiltration of microglial cells) in lobules VIII–X of the cerebellar vermis and to lesser extent in other lobules (Fig. S4 *D* and *H*). We also examined the abundance and morphology of neurons in affected regions by Golgi staining and found a clear reduction of Golgi-stained neurons in the FN, cerebellar vermis, and VN (Fig. S4 *I–N*). Residual Purkinje cells in late-stage KO mice showed abnormal dendritic arbors (Fig. S4 *R* and *S*) compared with CT mice (Fig. S4*Q*). Gallyas silver staining, an indicator of neurofibrillary tangles and other inclusions, showed prominent staining in large neurons in the VN (Fig. S4 *O* and *P*); likewise, granule cells and some Purkinje cells in lobe X of the cerebellum were intensely stained (Fig. S4 *T* and *U*). These results were confirmed with FluoroJade staining, another marker of neurodegeneration (Fig. S4 *V–Y*). Purkinje cell death is likely to be secondary to dysregulation within cerebellar circuits because selective inactivation of *Ndufs4* in Purkinje cells (as described in *Methods*) did not lead to overt pathology or behavioral abnormality in mice up to 8 mo of age.

No evidence of demyelination or oligodendrocyte pathology was detected with Luxol Fast Blue staining, antisera against cyclic nucleotide phosphodiesterase or myelin basic protein (Fig. S5 *A–C* and *E–G*). Likewise, normal labeling with an antiperipherin suggested that cranial nerves were unaffected (Fig. S5 *D* and *H*). No evidence of significant neuronal activation was observed in sections from KO mice using antisera against Fos. Because mitochondrial dysfunction might lead to reduction in ATP and accumulation of AMP, we performed immunolabeling for phosphorylated AMP kinase and phosphorylated acetyl CoA-carboxylase (an AMPK substrate) in brains from two KO mice, but we did not detect activation of either enzyme.

**Abnormal Mitochondria and Neuronal Degeneration in Affected Brain Regions of KO Mice.** In the VN, FN, OB, and posterior cerebellar vermis, as well as other areas before spongiform degeneration (i.e., anterior cerebellar vermis), abnormal mitochondria with compact and/or swollen cristae were found in nerve terminals of KO mice (Fig. 5 and Fig. S6). In the cerebellum, abnormal mitochondria predominated in presynaptic termini of molecular layer interneurons including basket cells surrounding Purkinje cell bodies (Fig. 5 *C* and *D*) and mossy fibers of the granular layer (Fig. S6*A*). In the lateral VN and FN, mitochondria with collapsed cristae were less prevalent but were observed in nerve terminals, some myelinated axons, primarily in axonal termini that appeared otherwise healthy, and occasional neuronal cell bodies (Fig. S6 *B, C,* and *I*).

Spongiform lesions observed by light microscopy in the VN, FN, and posterior cerebellar vermis of KO mice (Fig. 1 and 5*B* and Fig. S6*D*) corresponded ultrastructurally with degenerating nerve terminals (Fig. S6*B*). In the cerebellar vermis, the majority of these foci were located in the molecular and superficial granular cell layers of the nodulus and uvula. Most resembled either swollen dendrites, which made contact with presynaptic nerve terminals and contained degenerating organelles, or lucent extracellular spaces filled with granular and membranous debris left behind from degenerated neuronal processes. Ultrastructural evidence of cell soma degeneration was noted in rare Golgi cells of the cerebellar nodulus, scattered neurons in the FN (Fig. S6 *F* and *G*), and abundant neurons in the outer plexiform layer

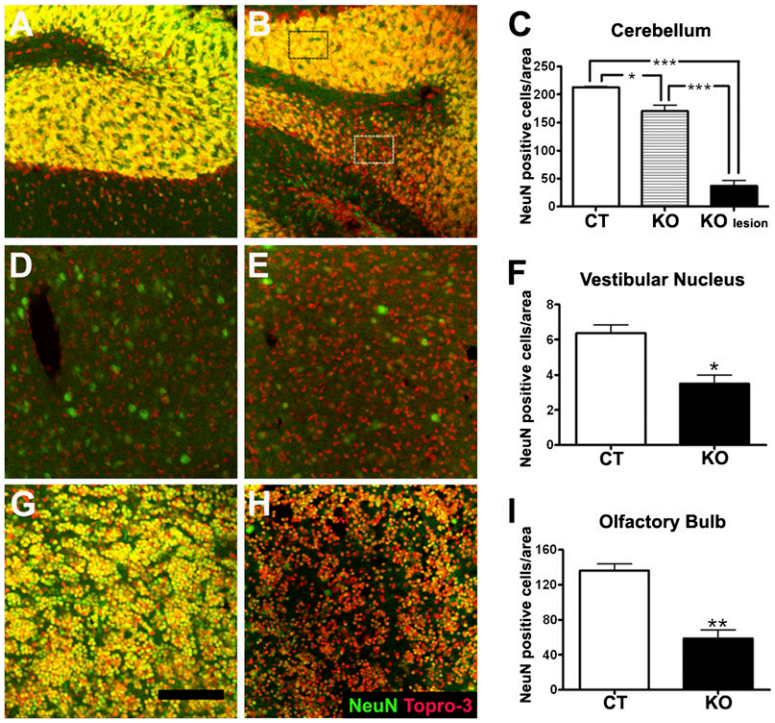


**Fig. 3.** Neuronal loss in affected brain areas of KO mice. (*A–C*) NeuN labeling (green) and Topro-3 counterstain (red) in the cerebellum of CT (*A*) and late-stage KO (*B*) mice. Colocalization of both labels is shown in yellow. (*C*) Quantification of NeuN-positive cells; the number of cells was reduced in lesion foci (KO lesion, representative area denoted by white rectangle), as well as in adjacent regions of the cerebellum (KO, black rectangle) of late-stage KO mice (*B*) compared with CT mice (*A*). *$P < 0.05$,*** $P < 0.001$ vs. CT. Topro-3–positive/NeuN-negative cells (probably microglia) were increased in lesioned areas of KO mice (*B*) (*D–F*) Significant decrease in NeuN-positive cells in the VN of KO mice (*E*) compared with CT mice (*D* and *F* for quantification), *$P < 0.05$ vs. CT. (*G–I*) Loss of NeuN-positive cells in the OB of late-stage KO mice (*H*) compared with CT mice (*G*, quantification in *I*). An increase in Topro-3–positive/NeuN-negative cells was observed in the OB of KO mice (*H*). **$P < 0.01$ vs. CT. (Scale bar, *A–H*, 100 μm.)

of the OB (Fig. 5*E* and Fig. S6*J*), which contained membranous and granular debris, as well as either swollen (Fig. 5*E*) or collapsed mitochondria (Fig. S6 *K–M*). The degenerating neurons in the OB corresponding to sites of caspase-3 activation and microglial infiltration were accompanied by microglial cells filled with lysosomal debris (Fig. S6*N*).

***Ndufs4* Gene Inactivation in Adult Mice.** To ascertain whether the fatal encephalopathy that develops in KO mice depends on absence of Ndufs4 during development of the CNS, we inactivated the *Ndufs4* gene in adult mice. We bred *Ndufs4*$^{lox/lox}$ mice with mice bearing a Cre recombinase gene (*Ubc-CreERt2*) that is induced in most cells by tamoxifen. These mice also expressed a G (t)*Rosa26Sor-lacZ* gene that is activated by Cre recombinase. After tamoxifen treatment at ~P60, most, but not all, brain regions revealed extensive expression of the reporter gene (Fig. S7 *A* and *B*). We used Southern blot analysis to determine the extent of *Ndufs4* gene recombination: >80% of the *Ndufs4* alleles recombined in most brain regions (Fig. S7*C*). Western blots revealed large decreases in the abundance of Ndufs4 protein as

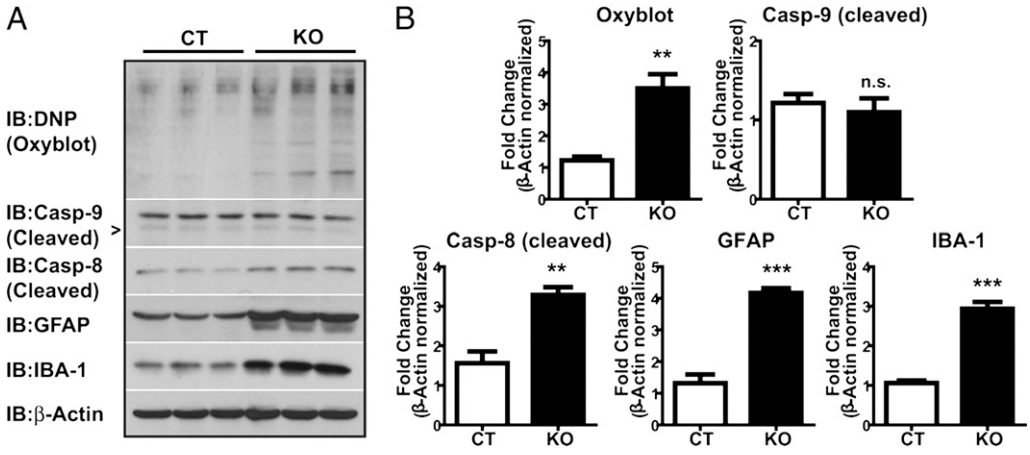


**Fig. 4.** Oxidative stress and caspase-8 OB of KO mice. (*A*) Western blot analysis of protein carbonylation (Oxyblot), active caspase-9, active caspase-8, GFAP, and Iba-1 levels in OB of CT and KO mice. (*B*) Densitometric analysis of Western blot images in *A*. Integrated density values for each lane were normalized to β-actin and expressed relative to the lowest value in CT. ** $P < 0.01$, *** $P < 0.001$ vs. CT.

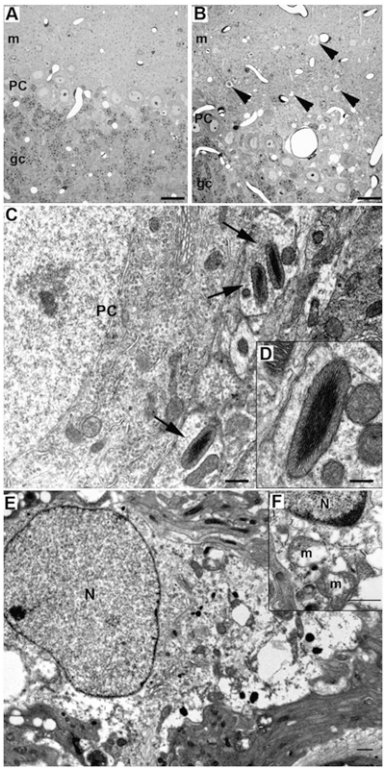


**Fig. 5.** Light microscopy and EM changes in cerebellar cortex and OB of KO Mice. (*A* and *B*) Light microscopy demonstrates granular (gc), Purkinje (PC), and molecular layers (m) in (*A*) anterior and (*B*) posterior vermis. Spongiform degeneration (arrowheads) is evident only in the posterior lobules, in addition to vascular spaces, which exist in both areas. (*C*) Abnormal mitochondria with compact cristae (arrows; higher magnification in *D*) are present in presynaptic basket cell nerve termini adjacent to the cell body of a Purkinje cell (PC). (*E*) Intracellular edema with swelling and lysis of cytoplasmic organelles is evident in a degenerating neuronal cell body (N, nucleus) from the periglomerular external plexiform layer of the OB. (*F, Inset*) Swollen mitochondria (m) and a portion of a nucleus (N) at higher magnification. (Scale bars, *A*, 35 μm; *B*, 35 μm; *C*, 1 μm; *D*, 0.5 μm; *E*, 1 μm; *F*, 1 μm.)

well (Fig. S7*D*). Seven months after the tamoxifen treatment, the mice were hypoactive (Fig. S7*E*), performed poorly on a rotarod (Fig. S7*F*), sometimes clasped their hindlimbs, occasionally gasped, and did not respond normally to hypoxia. These behavioral phenotypes resemble the early stage of complete KO mice and were associated with a mild degree of gliosis (Fig. S7*B*).

## Discussion

The phenotype of Ndufs4-null mice resembles that of humans with mutations in mitochondrial genes or nuclear genes encoding subunits of complex I, proteins important for assembly of mitochondrial complexes, or subunits of pyruvate dehydrogenase. Mutations in all of these genes impair mitochondrial respiration and are responsible for development of LS. Complex I deficiency in LS is not restricted to the brain but is usually detected in other tissues as well (4, 14, 20). However, LS patients primarily experience dysfunction of the CNS, reflected in MRI experiments and in the characteristic symptoms. Likewise, the Ndufs4 KO mice presented with growth deficiency, developmental delay, hypothermia, ataxia, respiratory abnormalities and defects in vision, all attributable to a CNS disorder. Although there are many similarities, a striking difference in the CNS phenotype of the mice studied here and LS is that the basal ganglia appear to be unaffected in the KO mice. The predominant role of the CNS in the phenotype of KO mice was confirmed by inactivation of Ndufs4 gene only in the CNS. Because the NesKO mice showed a phenotype essentially identical to the systemic KO mice, we have provided strong evidence for the neurological origin of the phenotype in these mice and, by extension, to LS. However, as a cautionary note, *Nestin-Cre* activates reporter-gene expression in a few cells in other organs including muscle-nerve bundles and skeletal muscle. Therefore, we cannot rule out a small contribution of peripheral Ndufs4 deficiency to the observed phenotype. We have not observed gliosis in the spinal cord of KO mice, and our previous analysis of KO mice revealed minimal alterations in muscle histology, physiology and metabolism (18); these results support encephalopathy as the primary cause of death in KO mice.

Mice and humans lacking Ndufs4, one of the 45 subunits of mitochondrial complex I, fail to thrive but the cause of death remains uncertain. Ndufs4 is not directly involved in electron transport within complex I, but is thought to play an important role in the assembly and/or stability of the complex (18) and may play a regulatory role because it can be phosphorylated (21). The phenotype that develops in the absence of Ndufs4 is complex, as expected for a protein that is presumably expressed in all cells. Why the neuropathology is restricted to just a few brain regions, assuming that microglial activation is a reliable marker of aberrant neuronal function, remains a mystery. Neurons in the OB, VN, and posterior lobules of the cerebellar vermis appear to be most vulnerable. Although many Purkinje cells in lobules VIII, IX, and X of the cerebellum ultimately die, the primary defect does not appear to be the Purkinje cells themselves because mitochondria in Purkinje cells appear normal whereas many mitochondria in neuronal processes that impinge on them often have collapsed cristae. Furthermore, mice lacking Ndufs4 selectively in Purkinje cells manifest mild behavioral and neuropathological consequences. These observations lead us to conclude that Purkinje cells die either because of dysregulation of cerebellar circuitry, most likely cerebellar granule cells or projections from the VN and IO, or because of their hypersensitivity to hypoxia (22). Cerebellar defects alone are sufficient to cause ataxia, but they rarely cause death (23–25).

We looked for LS-like neuropathology in the brains of KO and NesKO, and correlated the findings with disease manifestation and progression. Light microscopy and EM changes in specific brain regions of mice corresponded to deteriorating performance in behavioral and physiological assays. The degree of gliosis closely matched the severity of disease. Ataxia, hypothermia, and general morbidity increased in tandem with the emergence of microglial activation and lesions within the brainstem and cerebellum. The observation of increasingly severe gliosis in the cerebellum, dorsomedial medulla (FN and VN), and occasionally in the ventral medulla suggests that dysregulation within these regions is responsible for the escalating ataxia of the KO mice.

The presence of glial activation can represent either the cause or the consequence of cell death. Hence, we characterized the cellular mechanisms underlying the pathology of KO mice. We observed caspase-8 activation in affected areas of KO mice; this caspase initiates the extrinsic (death-receptor–mediated) apoptotic pathway (26), suggesting a role of cytokines released from activated glial cells in the neural pathology. The lack of activated caspase-9, the main initiator of the intrinsic (mitochondrial) apoptotic pathway (27), further suggests that neuronal death in KO mice was initiated by activated glial cells. The increase in carbonyl groups is indicative of protein oxidation by reactive oxygen species (ROS), which may be caused by glial activation. However, complex I dysfunction per se may contribute to the presence of ROS, which can activate glial cells (28). Activation of caspase-8 suggests that apoptosis is initiated; however, we failed to see significant activation of caspase-3 (the main effector caspase) in KO mice. Normal ATP levels have been shown to be necessary for the culmination of apoptotic cell death (29, 30),

and ATP depletion leads to a switch from apoptosis to necrosis in several paradigms (29–32). Thus, low ATP production due to mitochondrial complex I dysfunction may abrogate apoptosis and result in necrotic death instead. Ultrastructural analysis in affected areas of KO mice revealed extensive indications of necrotic cell death whereas apoptotic cell death was rarely detected. Therefore, our working hypothesis is that complex I dysfunction triggers the release of cellular signals that activate glial cells. This activation leads to oxidative stress, cytokine release by microglia, and activation of the extrinsic apoptotic pathway in neurons, which, with insufficient ATP, gives way to a necrotic cell death.

We also show that LS-like phenotype of the KO mice is not strictly a developmental phenomenon by demonstrating that inactivation of the *Ndufs4* gene in adult animals also leads to early-stage phenotype. We suspect that the phenotype is mild compared with that of KO or NesKO mice because of incomplete recombination (80–90%) despite 10 d of tamoxifen treatment. Some brain regions have virtually no recombination (e.g., granule cell layers in OB and cerebellum) based on Xgal staining, which is consistent with the Southern and Western blot results. However, it is also possible that more severe neuronal damage occurs during development in the absence of Ndufs4.

Our results validate the usefulness of the conditional *Ndufs4* KO mouse as a model to study the mechanisms of neurodegeneration due to mitochondrial dysfunction. The results have obvious implications for understanding the progression of symptoms in LS. Selective inactivation of *Ndufs4* in select neuronal populations, or restoration in specific brain regions, promises to provide even more resolution to this complicated syndrome.

## Methods

**Animals.** Ndufs4-null mice (KO) were generated as described elsewhere (18). The NesKO mice were made by crossing the conditional Ndufs4 mice with *Nestin-Cre* mice. *Pcp2-Cre* mice and *Ubc-CreERt2* mice were used to inactivate Ndufs4 in Purkinje cells or in the adult by administration of tamoxifen, respectively (*SI Methods*). All animal experiments were approved by the Animal Care and Use Committee at the University of Washington. Mice were maintained with rodent diet (5053; Picolab) and water available ad libitum with 12-h light–dark cycle at 22 °C.

**Behavioral Assays.** Details of visual placement/touch response, light/dark exploration, and rotarod tests can be found in *SI Methods.* Behavioral tests are listed in Table S1 (details available upon request).

**Mitochondrial Assays.** Mitochondrial activity assays were performed as described before (18) and in *SI Methods.*

**Histology, Immunofluorescence, and EM.** Mice at different stages of disease were anesthesized with an overdose of pentobarbital, perfused with PBS, followed by 4% paraformaldehyde (PFA). Tissue sections were cut and subjected to H&E, Luxol Fast Blue, Gallyas silver, Golgi, X-Gal, or FluoroJade C staining by standard methods. Either 8-μm paraffin sections or 30-μm free-floating sections were used for immunofluorescence with primary antibodies to the following: GFAP, laminin, CNPase, or caspase 3 or 8, phosphorylated AMPK or acetyl-CoA carboxylase, Iba-1-cfos, peripherin, myelin basic protein, calbindin; CD11b or NeuN. Sources of antibodies, dilutions, and visualization details can be found in *SI Methods.* EM was performed by standard techniques (*SI Methods*).

**Western, Oxyblot, and Southern Blot.** Western blots for Ndufs4, cleaved caspase-9, cleaved caspase-8, and GFAP were performed as decribed elsewhere (33) and in *SI Methods.* Protein oxidation was assessed using an Oxyblot detection kit. For Southern blot analysis of the *Ndufs4* gene, DNA from cerebellum, brainstem, or fore/hindbrain was digested with BspHI, electropohoresed on 1.0% agarose gels, transferred to nylon membrane, and hybridized with a unique probe that would distinguish *Ndufs4*$^{+}$, *Ndufs4*$^{lox}$, and *Ndufs*$^{\Delta}$ alleles.

**ACKNOWLEDGMENTS.** We thank Glenda Froelick for histology and Nora Meneses for help maintaining the mouse colony. Research was supported in part by the Seattle Children's Mitochondria Research Guild (R.D.P.) and the Spanish Ministry of Science and Innovation (A.Q. and E.S).

1. Chol M, et al. (2003) The mitochondrial DNA G13513A MELAS mutation in the NADH dehydrogenase 5 gene is a frequent cause of Leigh-like syndrome with isolated complex I deficiency. *J Med Genet* 40:188–191.
2. Leigh D (1951) Subacute necrotizing encephalomyelopathy in an infant. *J Neurol Neurosurg Psychiatry* 14:216–221.
3. Rahman S, et al. (1996) Leigh syndrome: Clinical features and biochemical and DNA abnormalities. *Ann Neurol* 39:343–351.
4. Munaro M, et al. (1997) A single cell complementation class is common to several cases of cytochrome c oxidase-defective Leigh's syndrome. *Hum Mol Genet* 6:221–228.
5. Piao YS, Tang GC, Yang H, Lu DH (2006) Clinico-neuropathological study of a Chinese case of familial adult Leigh syndrome. *Neuropathology* 26:218–221.
6. Arii J, Tanabe Y (2000) Leigh syndrome: Serial MR imaging and clinical follow-up. *AJNR Am J Neuroradiol* 21:1502–1509.
7. Debray FG, Lambert M, Lortie A, Vanasse M, Mitchell GA (2007) Long-term outcome of Leigh syndrome caused by the NARP-T8993C mtDNA mutation. *Am J Med Genet A* 143A:2046–2051.
8. Desguerre I, et al. (2003) Infantile spasms with basal ganglia MRI hypersignal may reveal mitochondrial disorder due to T8993G MT DNA mutation. *Neuropediatrics* 34: 265–269.
9. Nagashima T, et al. (1999) Adult Leigh syndrome with mitochondrial DNA mutation at 8993. *Acta Neuropathol* 97:416–422.
10. Wick R, Scott G, Byard RW (2007) Mechanisms of unexpected death and autopsy findings in Leigh syndrome (subacute necrotising encephalomyelopathy). *J Forensic Leg Med* 14:42–45.
11. Barkovich AJ, Good WV, Koch TK, Berg BO (1993) Mitochondrial disorders: Analysis of their clinical and imaging characteristics. *AJNR Am J Neuroradiol* 14:1119–1137.
12. Lee HF, Tsai CR, Chi CS, Lee HJ, Chen CC (2009) Leigh syndrome: Clinical and neuroimaging follow-up. *Pediatr Neurol* 40:88–93.
13. Lebon S, et al. (2003) Recurrent de novo mitochondrial DNA mutations in respiratory chain deficiency. *J Med Genet* 40:896–899.
14. Loeffen J, et al. (1998) The first nuclear-encoded complex I mutation in a patient with Leigh syndrome. *Am J Hum Genet* 63:1598–1608.
15. Cavanagh JB, Harding BN (1994) Pathogenic factors underlying the lesions in Leigh's disease. Tissue responses to cellular energy deprivation and their clinico-pathological consequences. *Brain* 117:1357–1376.
16. Cooper MP, et al. (2006) Defects in energy homeostasis in Leigh syndrome French Canadian variant through PGC-1alpha/LRP130 complex. *Genes Dev* 20:2996–3009.
17. Ostergaard E, et al. (2007) Mitochondrial encephalomyopathy with elevated methylmalonic acid is caused by SUCLA2 mutations. *Brain* 130:853–861.
18. Kruse SE, et al. (2008) Mice with mitochondrial complex I deficiency develop a fatal encephalomyopathy. *Cell Metab* 7:312–320.
19. Tronche F, et al. (1999) Disruption of the glucocorticoid receptor gene in the nervous system results in reduced anxiety. *Nat Genet* 23:99–103.
20. Merante F, et al. (1993) A biochemically distinct form of cytochrome oxidase (COX) deficiency in the Saguenay-Lac-Saint-Jean region of Quebec. *Am J Hum Genet* 53: 481–487.
21. Papa S, et al. (2001) Mutation in the NDUFS4 gene of complex I abolishes cAMP-dependent activation of the complex in a child with fatal neurological syndrome. *FEBS Lett* 489:259–262.
22. Welsh JP, et al. (2002) Why do Purkinje cells die so easily after global brain ischemia? Aldolase C, EAAT4, and the cerebellar contribution to posthypoxic myoclonus. *Adv Neurol* 89:331–359.
23. Glickstein M (1994) Cerebellar agenesis. *Brain* 117:1209–1212.
24. Timmann D, Dimitrova A, Hein-Kropp C, Wilhelm H, Dörfler A (2003) Cerebellar agenesis: Clinical, neuropsychological and MR findings. *Neurocase* 9:402–413.
25. Titomanlio L, Romano A, Del Giudice E (2005) Cerebellar agenesis. *Neurology* 64:E21.
26. Wajant H (2002) The Fas signaling pathway: More than a paradigm. *Science* 296: 1635–1636.
27. Allan LA, Clarke PR (2009) Apoptosis and autophagy: Regulation of caspase-9 by phosphorylation. *FEBS J* 276:6063–6073.
28. Block ML, Zecca L, Hong JS (2007) Microglia-mediated neurotoxicity: Uncovering the molecular mechanisms. *Nat Rev Neurosci* 8:57–69.
29. Ferrari D, Stepczynska A, Los M, Wesselborg S, Schulze-Osthoff K (1998) Differential regulation and ATP requirement for caspase-8 and caspase-3 activation during CD95- and anticancer drug-induced apoptosis. *J Exp Med* 188:979–984.
30. Hartmann A, et al. (2001) Caspase-8 is an effector in apoptotic death of dopaminergic neurons in Parkinson's disease, but pathway inhibition results in neuronal necrosis. *J Neurosci* 21:2247–2255.
31. Leist M, Single B, Castoldi AF, Kühnle S, Nicotera P (1997) Intracellular adenosine triphosphate (ATP) concentration: A switch in the decision between apoptosis and necrosis. *J Exp Med* 185:1481–1486.
32. Eguchi Y, Shimizu S, Tsujimoto Y (1997) Intracellular ATP levels determine cell death fate by apoptosis or necrosis. *Cancer Res* 57:1835–1840.
33. Sanz E, et al. (2009) Cell-type-specific isolation of ribosome-associated mRNA from complex tissues. *Proc Natl Acad Sci USA* 106:13939–13944.